Oroval, M.; Díez, P.; Aznar, E.; Coll Merino, MC.; Marcos Martínez, MD.; Sancenón Galarza, F.; Villalonga, R.... (2017). Self-Regulated Glucose-Sensitive Neoglycoenzyme-Capped Mesoporous Silica Nanoparticles for Insulin Delivery. Chemistry - A European Journal. 23(6):1353-1360. https://doi.org/10.1002/chem.201604104

Self-regulated glucose-sensitive neoglycoenzyme-capped mesoporous silica nanoparticles for insulin delivery

Mar Oroval,[a],[b] Paula Díez ,[c],[d] Elena Aznar,[b],[a] Carmen Coll, [a],[b] María Dolores Marcos,[a],[b],[e] Félix Sancenón,[a],[b],[e] Reynaldo Villalonga[c],[d] and Ramón Martínez-Máñez*[a],[b],[e]

Abstract: We describe herein the preparation of glucose-sensitive capped mesoporous silica nanoparticles for insulin delivery. The new material consists of an expanded pore nanometric silica support grafted with 1-H-propyl-1-H-benzimidazole groups, loaded with fluorescein isothiocyanate-labeled insulin (FITC-Ins) and capped by the formation of inclusion complexes between CD-modified-glucose oxidase (CD-GOx) and the benzimidazole groups grafted on the mesoporous support. Insulin delivery from the gated material in simulated blood plasma was assessed upon addition of glucose. Glucose is transformed by GOx into gluconic acid that promoted the dethreating of the benzimidazole-CD-GOx inclusion complexes allowing cargo release. Small quantities of this support would be needed to release the amount of insulin necessary to decrease diabetic blood glucose concentration to the regular level.

Introduction

Hybrid organic-inorganic nanomaterials have attracted significant interest due to their unique properties resulting from the combination of organic and bioorganic chemistry and material science.[1] In this field, the design and synthesis of mesoporous hybrid gated materials, with the ability to be selectively opened upon the application of an external stimulus and release an entrapped cargo, has generated special interest to the scientific community in recent years.[2-5] These gated materials are composed of two main subunits: (i) a porous scaffold in which a certain cargo is stored and (ii) molecular, supramolecular or biomolecular entities grafted onto the outer surface, which allow control delivery of the entrapped payload.[6,7] Mesoporous silica nanoparticles (MSNs) have been widely used as inorganic support in the construction of gated nanodevices. MSNs present some remarkable features as they are mechanically hard, biocompatible, ease to functionalize using well-known chemistries, have a high loading capacity and tunable pore size.[8–10] In fact, numerous controlled-release systems using mesoporous silica supports have been described using physical,[11-14] chemical[15-17] or biochemical[18-21] stimuli.

From different point of view, diabetes mellitus is a chronic metabolic disease characterized by an accumulating concentration of glucose in blood and urine. This illness, which requires ongoing medical care and patient self-management, takes place when beta cells of pancreas fail to produce insulin (type 1) or produce it insufficiently to overcome insulin resistance in target tissues (type 2).[22] Moreover, it is a major leading cause of mortality in industrialized countries, leading to severe complications, such as kidney disease, retinopathy, neuropathy, leg or foot amputations and heart diseases.[23] In healthy humans, the concentration of glucose in blood is controlled in a finely regulated manner to maintain glucose between 3.5 and 7 mM.[24] In diabetic patients, administration of insulin to help the body to use or store the blood glucose obtained from food is essential in type 1 and longstanding type 2 diabetes patients, requiring continuous dose adjustments based on self-monitoring of blood glucose levels. This widely used therapy is not exempt of hazards. The most important risk when treating with insulin is hypoglycemia.[25] Extremely low blood sugar levels can be life-threatening resulting in seizures, nervous system damage and even comma. Thus, a perfect insulin therapy should minimize the risk of hypoglycemia while improving glycemic control. In this context, the design systems able to detect fluctuations in blood glucose concentrations and release insulin in a self-regulated fashion is highly desirable and still a challenge.[26–28]

In this context different strategies integrated with a large variety of chemical approaches for insulin delivery in response to glucose concentration changes have been reported.[29-39] Nevertheless, only few MSNs based systems have been described for this purpose. One of the first reported examples was developed by Lin et al.,[40] that used MSNs capped with gluconic acid-modified insulin (G-Ins) and loaded with cyclic adenosine monophosphate (cAMP). The nanomaterial demonstrated to be glucose-sensitive, releasing both G-Ins and cAMP. Moreover, Shi and co-workers reported an insulin loaded mesoporous silica particles coated with GOx enzyme-multilayers that were cross-linked with glutaraldehyde and acted as gatekeepers. In the presence of glucose, GOx generated gluconic acid with a subsequent decrease in the environment pH. As a consequence, the enzyme multilayer was expanded and the entrapped insulin released.[41] Another example was recently developed by Asefa and co-workers who described the preparation of MSNs for insulin release by tethering insulin molecules onto boronic acid functionalized MSNs and then coating the material with a shell of the pH-sensitive polymer polyacrylic acid.[42] The material exhibited both pH- and glucose-dependent release of insulin.

[a] M. Oroval, Dr. E. Aznar, Dr. C. Coll, Dr. M.D Marcos, Dr. F. Sancenón, Prof. R. Martínez-Máñez
Instituto Interuniversitario de Investigación de Reconocimiento Molecular y Desarrollo Tecnológico. Unidad Mixta Universitat Politècnica de València - Universitat de València. Camino de Vera s/n, 46022, Valencia, Spain
[b] M. Oroval, Dr. E. Aznar, Dr. M.D Marcos, Dr. F. Sancenón, Prof. R. Martínez-Máñez
CIBER de Bioingeniería, Biomateriales y Nanomedicina (CIBER-BBN)
[c] P Díez, Dr. R. Villalonga
Department of Analytical Chemistry, Faculty of Chemistry, Universidad Complutense de Madrid, Madrid (Spain)
[d] P Díez, Dr. R. Villalonga
IMDEA Nanoscience, Cantoblanco Universitary city, Madrid (Spain)
[e] Dr. M.D Marcos, Dr. F. Sancenón, Prof. R. Martínez-Máñez
Departamento de Química, Universitat Politècnica de València, Camino de Vera s/n, 46022 València, Spain

Based in these concepts and considering the multiple advantages of MSNs as carriers in controlled release applications,[43–45] we report herein the design of a new self-regulated glucose-sensitive platform for insulin release. Our strategy relies on the use of β-cyclodextrin-modified enzyme glucose oxidase (CD-GOx) as gatekeeper in MSNs and the enzymatic reaction between glucose and GOx as trigger which induces insulin delivery.[46] This approach is simple and present some advantages versus other reported glucose-triggered insulin release, such as the storage of insulin into the pores preventing its degradation.

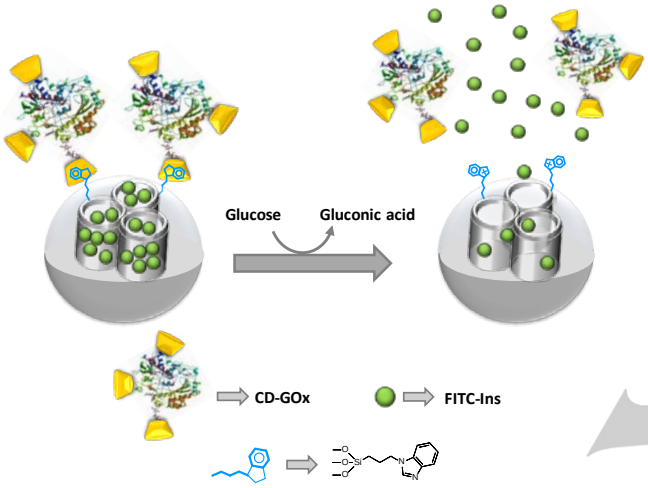

Scheme 1. Schematic representation of the glucose-triggered FITC-Ins release from nanodevice **S3**.

Results and Discussion

The glucose-responsive nanomaterial.

The designed nanodevice for controlled insulin release is shown in Scheme 1. The system consists of MSNs with large pores loaded with fluorescein isothiocyanate-labeled insulin (FITC-Ins), functionalized on the outer surface with 1-propyl-1-H-benzimidazol groups and capped by CD-GOx via the formation of inclusion complexes between benzimidazol groups in the pore outlets and β-cyclodextrin groups from CD-GOx (solid **S3**). When **S3** is placed in an aqueous medium, addition of glucose is expected to trigger insulin delivery. Glucose is recognized by glucose oxidase enzyme and hydrolyzed into gluconic acid (pK_a=3.6). The generation of gluconic acid induces a local drop in pH that would cause the protonation of benzimidazol groups (pK_a=5.55) on **S3** and the dethreading of the inclusion complexes between benzimidazol and CD-GOx, finally resulting in the delivery of entrapped insulin yielding solid **S4**.

MSNs with large pores were prepared by the two-step swelling incorporation method, following previous reports with some modifications.[47,48] Especifically, tetramethylorthosilicate (TMOS) and cetyltrimethylammonium bromide (CTAB) were used as the inorganic precursor and structure directing agent, respectively to obtain a nanoparticulated and mesostructured material (**S0-1**). In a second step, material **S0-1** was subjected to a hydrothermal treatment in the presence of equal volumes of 1,3,5-trimethylbenzene (TMB), water, and ethanol to achieve the pore expansion (**S0-2**). Then the surfactant and the pore expanding agent (TMB) were removed by calcination to obtain the final support **S0-3**. The calcined nanoparticles were grafted with 3-iodopropyltrimethoxysilane and the resulting material was treated with benzimidazole yielding solid **S1** which contains 1-propyl-1-H-benzimidazole groups in the surface. Subsequently, the pores were loaded with FITC-Ins by a diffusion process to give solid **S2**. Finally, the support was capped by the addition of CD-GOx to a suspension of **S2** in water at pH 7.5 to yield the final capped solid **S3**, which was centrifuged and carefully washed with water at pH 7.5.

Materials characterization.

The prepared materials were characterized using standard procedures. The powder X-ray diffraction (PXRD) pattern of solids **S0-1**, **S0-2**, **S0-3**, **S1** and **S2** are shown in Figure 1. As observed, the PXRD pattern of the as-synthesized nanoparticles **S0-1** (Figure 1, curve a) shows the three typical low-angle reflections of a hexagonal-ordered matrix that can be indexed as (100), (110) and (200) Bragg peaks. However, the regularity of mesopores was highly diminished after pore expansion due to the reorganization of the internal mesostructure, which is corroborated by the significant broadening and the clearly observed displacement of the (100) peak to lower 2θ values (0.976°) (Figure 1, curve b, solid **S0-2**). In addition, diffraction peaks assignable to the (110) and (200) planes disappeared. On the other hand, the condensation of silanol groups during the calcination step is reflected in a slight shift of the (100) peak to higher 2θ values (1.094°) (Figure 1, curve c, solid **S0-3**), corresponding to an approximate cell contraction of 11.3 Å. The a_0 cell parameter for **S0-3** was calculated to be 93.13 Å (d_{100}= 80.65 Å). Finally, curves d and e in Figure 1, correspond to the PXRD pattern of **S1** and **S2**. The presence of the (100) peak in these solids indicated that besides surface functionalization and pore loading, the porous structure in the nanoparticles is preserved.

By means of transmission electron microscopy (TEM) analysis the porous structure, particle size and morphology of the different samples was also studied. Figure 2 shows a representative image of the calcined scaffold **S0-3**, **S1**, **S2**, **S3** and **S4** materials. It can be clearly seen that these nanoparticles show a spherical form with diameters ranging from 200 to 300 nm. TEM images of **S1**, **S2** and **S3**, also evidence that porosity is still retained after functionalization with 1-propyl-1-H-benzimidazole, loading with FITC-Ins and capping with CD-GOx (Figure 2 b, c, d). Moreover, the TEM representative image of solid **S4** (Figure 2f) confirms that the particle morphology and the porous network remained unaltered after delivery of FITC-Ins and the detachment of CD-GOx from the surface. In addition, particle size and morphology of solid **S3** was also studied by field emission scanning electron microscopy (FSEM). Figure 2e confirms the spherical morphology and size of solid **S3** observed in TEM analysis (Figure 2 d).

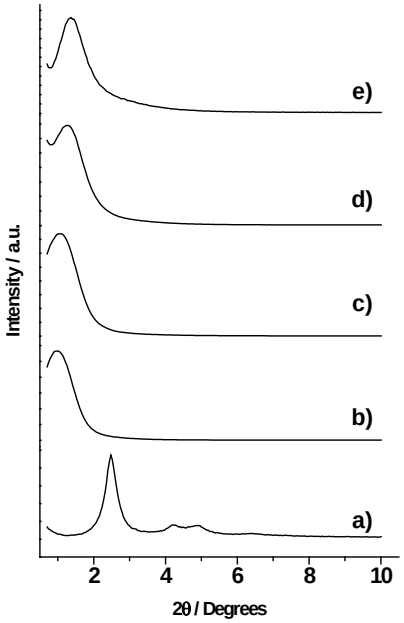

Figure 1. Powder X-ray diffraction patterns of a) as synthesised nanoparticles **S0-1**, b) pore expanded nanoparticles **S0-2**, c) pore expanded and calcined nanoparticles **S0-3**, d) solid **S1** containing 1-propyl-1-H-benzimidazole and e) solid **S2** containing 1-propyl-1-H-benzimidazole and loaded with FITC-Ins.

As a complement to PXRD and TEM, adsorption-desorption measurements were also carried out to study the porous structure of the calcined nanoparticles **S0-3** and solid **S2** (see Figure 3). Using the Barret-Joyner-Halenda (BJH)[49] model on the adsorption branch of the isotherm the pore diameter and pore volume were calculated (Table 1). Also, the specific surface was calculated by the application of the BET model.[50] The N_2 adsorption-desorption isotherms shown in Figure 3a (calcinated **S0-3** nanoparticles) shows that pore filling occurred over a large range of P/P_0 indicating a wide pore size distribution. On the other hand, the first adsorption step appears at relative high pressure values ($0.7 < P/P_0 < 0.8$) evidencing the existence of large pores. This step preserves a type-IV isotherm but with a clear H1 hysteresis loop. The total specific area was calculated to be 527 $m^2\ g^{-1}$, whereas the pore size distribution curve (Figure 3, inset) shows a very wide pore size distribution starting in 4 nm and extending up to 18.5 nm, with a mean value of *ca.* 11.8 nm. Futhermore, two shoulders at *ca.* 4.7 and 9.4 nm can also be appreciated.

On the other hand, a pore volume of 0.82 $cm^3\ g^{-1}$ and surface area of 302 $m^2 g^{-1}$ where determined for solid **S2** which means a lower N_2 adsorption when compared with the starting calcined material. Moreover, two main features can be appreciated in the pore size distribution of solid **S2**. One is the shift of the maximum towards smaller size values, as it can be expected from the filling of the pores. The second one is that the distribution becomes narrower in the area of smaller pores. This observation may be related with lower difficulty for the FITC-Ins molecules to abandon the solid from the wider pores when washing solid **S2** during the synthesis process. Hence, the smaller pores will remain fully filled while the big ones may still appear not completely blocked.

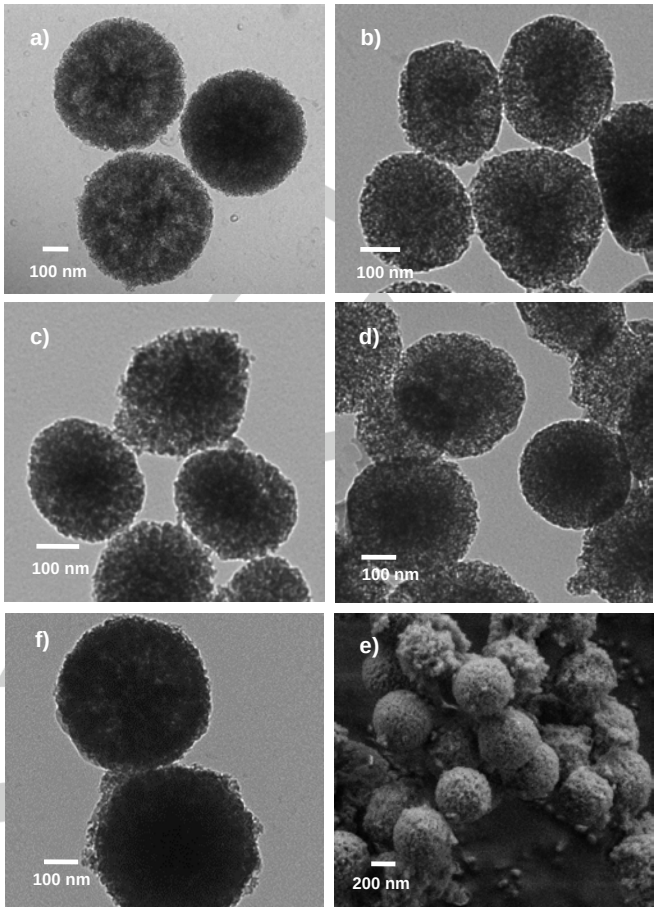

Figure 2. Representative TEM images of a) calcined nanoparticles, b) solid **S1**, c) solid **S2**, d) solid **S3** and e) solid **S4** showing the porosity of the silica-based nanomaterials. f) FSEM image of solid **S3** showing the spherical morphology of the nanoparticles.

Table 1. BET specific surface values, pore volumes and pore sizes calculated from the N_2 adsorption-desorption isotherms for selected materials.

Sample	S_{BET} ($m^2\ g^{-1}$)	Pore volume ($cm^3\ g^{-1}$)	Pore diameter (nm)
S0-3	527	1.26	11.8
S2	302	0.82	8.9

The particle size studies were completed by measuring the diameter of calcined nanoparticles **S0-3** and the hybrid materials **S2** and **S3** by dynamic light scattering (DLS) (Figure 4, and Table 2). All measurements were performed in triplicate on previously sonicated dispersions of the nanomaterials in simulated blood plasma at a concentration of 0.01 mg mL^{-1}. The Z potential was also determined. Functionalization with benzimidazol moieties and loading with FITC-Ins reduced the zeta potential of the nanoparticles **S2** (-26.5 mV) compared to that of calcined **S0-3** (-31.4 mV). For the final nanodevice **S3**, the surface charge was reduced even more (-17.7) compared to **S2** as a consequence of capping with CD-GOx. In addition an increase of the hydrodynamic diameter after each

functionalization step was observed which resulted in a hydrodynamic diameter of 426.1 nm for the final **S3** nanodevice (see Table 2).

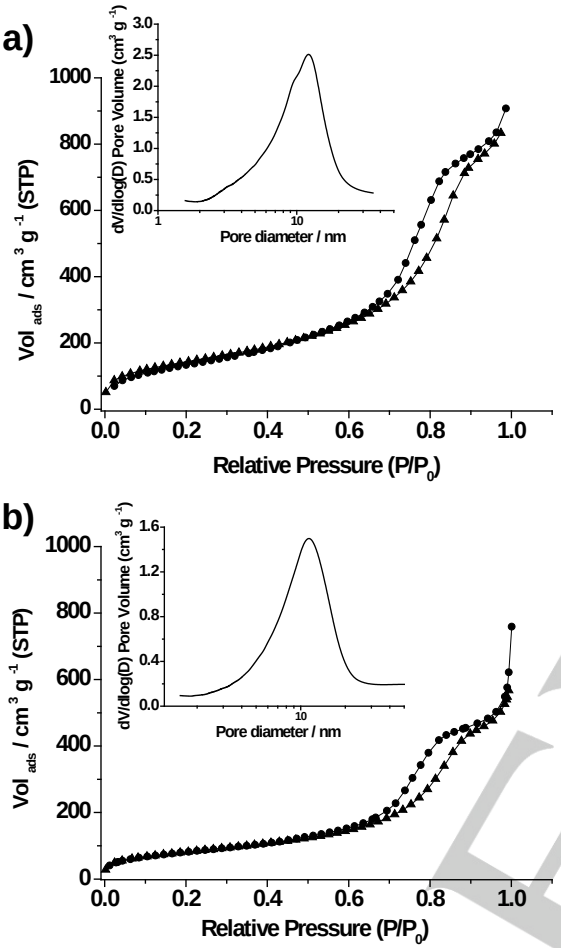

Figure 3. The nitrogen adsorption-desorption isotherms for a) calcined nanoparticles **S0-3** and b) **S2** material. Inset: pore size distribution of the calcined material.

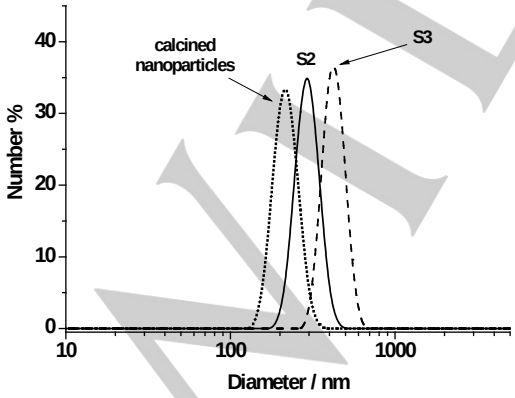

Figure 4. Particle size distribution by number of particles obtained by DLS studies for calcined nanoparticles **S0-3**, **S2** and **S3**.

Table 2. Diameter measured by DLS and surface zeta potential of calcined nanoparticles **S0-3**, **S2** and **S3** materials.

Sample	Particle diameter (nm)	Zeta potential (mV)
S0-3	237.9 ± 30.3	-31.4
S2	294.7 ± 41.4	-26.5
S3	426.1 ± 54.2	-17.7

Moreover, the content of 1-propyl-1-H-benzimidazole and FITC-Ins in **S1**, **S2** and **S3** were determined from thermogravimetric and elemental analysis and are detailed in Table 3. Besides, energy-dispersive X-ray spectroscopy (EDX) clearly showed the presence of C, N, O and Si atoms in these solids. In addition, with the aim to estimate the content of CD-GOx retained in the final solid **S3**, the absorbance of CD-GOx in the solution after the capping process was measured. The amount of CD-GOx in the solid **S3** was calculated to be $2.11 \cdot 10^{-3}$ mg g^{-1} SiO_2, representing 2 U of immobilized neoglycoenzyme per mg SiO_2 according to enzyme activity assays.

Table 3. Content of FITC-Ins and 1-propyl-1-H- benzimidazole in the prepared solids **S1**, **S2** and **S3** in mmol g^{-1} SiO_2.

Sample	$\alpha_{FITC\text{-}Ins}$	$\alpha_{1\text{-propyl-1-H-benzimidazole}}$
S1	-	1.24
S2	0.20	1.24
S3	0.17	1.24

Glucose-triggered controlled release of insulin.

This section evaluates the self-regulated insulin delivery from **S3** nanoparticles in the presence of glucose. As stated above, in humans, the concentration of this saccharide in blood is controlled by pancreas, which produces and delivers insulin in a finely regulated manner to maintain glucose between 3.5 and 7 mM.[24] The assessment of **S3** in a realistic competitive environment was accomplished by using simulated blood plasma. In a typical experiment, a suspension of **S3** was added to simulated blood plasma (pH 7.4) containing glucose at a concentration of 50 mM. At the same time a similar suspension of **S3** in the absence of glucose was used as control. Both suspensions were stirred for 20 h under dark and aliquots were separated at programmed times and centrifuged in order to remove the nanoparticles and isolate the supernatant. FITC-Ins release was determined by monitoring the fluorescence intensity in the solution (λ_{ex} = 495 nm; λ_{em} = 514 nm). Figure 5 shows the delivery profile of FITC-Ins from solid **S3** in the presence and in the absence of glucose as well as the the FITC-Ins efficiency release from **S3** in %. The results showed that solid **S3** was tightly capped and only a 3 % cargo was released after 20 h in the control experiment (see curve a in Figure 5). In contrast, the presence of 50 mM of glucose induced a remarkable cargo

delivery (ca. 26% of loaded FITC-Ins) from solid **S3** after 20 h (curve b). This observation confirms the proposed mechanism, in which the glucose oxidation to gluconic acid by the CD-GOx promotes cargo release. Also, it is worth mentioning that the spherical nanoparticle morphology and the porous structure persisted in solid **S4 r**egardless of the FITC-Ins delivery (Figure 2f).

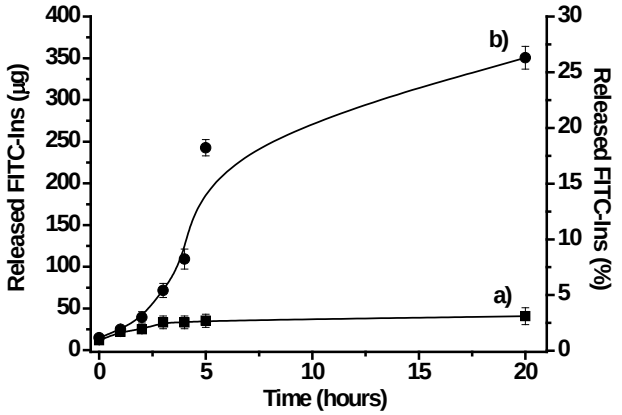

Figure 5. Amount of FITC-Ins released (left y axis) and FITC-Ins release efficiency (right y axis) from 1 mg of solid **S3** as a function of time in the absence (curve a) and in the presence of 50 mM of glucose (curve b).

A more in depth, study of cargo release profile from **S3** in the presence of glucose showed two different delivery trends. At shorter times, there was a quick release of insulin whereas at longer times the delivery was slower. In order to clarify these two different profiles the release kinetic in the presence of glucose at shorter times (0 to 4 hours) was fitted to the Higuchi model. Higuchi's model describes drug release as a diffusion process based in the Ficks's law and it is square root time dependent.[51] This extended model takes into account the hypotheses that initial cargo concentration in the matrix is much higher than cargo solubility, that diffusion takes place in only one dimension and that cargo diffusivity is constant. This model has been broadly and satisfactorily applied to describe drug release kinetics from porous matrices.[52,53] Figure 6 shows the fitting of the model to data taken in the first hours of the delivery (0 to 4 h). The good fitting observed suggested that FITC-Ins delivery from **S3** pores is essentially a diffusive process. At longer times a certain deviation from linearity was found (data not shown). This effect (two steps in the release profile) has also been described in other kinetic release studies of certain guests (usually drugs) from porous carrier materials.

As a step forward, the release of FITC-Ins from **S3** as a function of the glucose concentration was studied. In these experiments FITC-Ins delivered after 4 h from **S3** was studied in the glucose concentration range usually found in humans (i.e. up to 40 mM) (see Figure 7). The figure shows that in the presence of small amounts of glucose the delivered FITC-Ins is low. In contrast, when glucose concentration increased the capped system reacted delivering a high FITC-Ins dose mimicking healthy pancreas response.

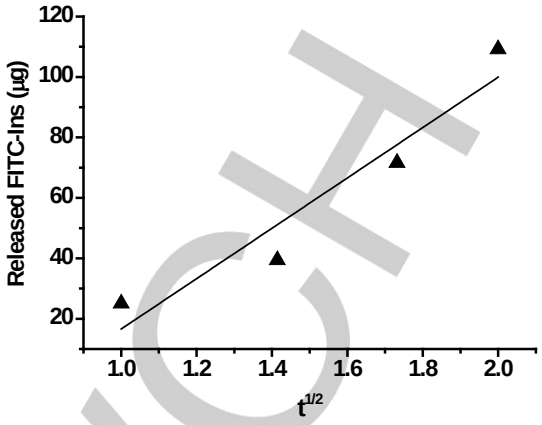

Figure 6. Amount of FITC-Ins delivered from solid **S3** vs. the square root of time (t) in simulated human blood plasma.

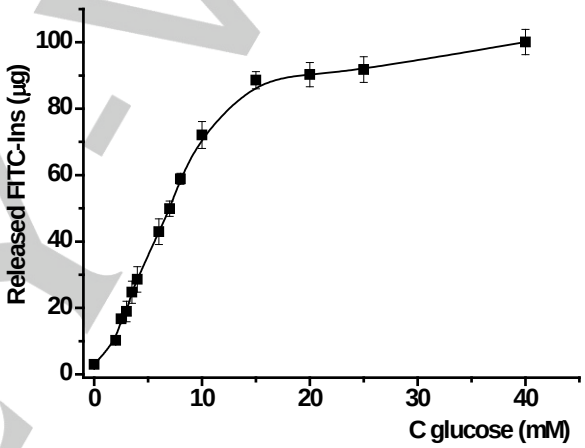

Figure 7. Amount of FITC-Ins released (left y axis) and FITC-Ins release efficiency (right y axis) from 1 mg of solid **S3** as a function of glucose concentration after 4h upon addition of the nanomaterial.

The World Health Organization defines diabetes mellitus when fasting plasma glucose level is higher than 126 mg/dL (7.0 mM) after the intake of 75 g of glucose.[55] This illness, if unmedicated, causes glucose peaks up to 40 mM, [56,57] especially after food intake. In a healthy person, to counteract this effect, blood insulin levels after eating rise more than 10-fold from a baseline of around 20-30 pM to 250-300 pM.[24] Taking into account that the average blood volume in an adult is 5 L, and that **S3** delivers ca. 5.91 x 10^{-9} mol of Ins per mg, (after 2.5 h for a concentration of glucose 50 mM) it can be estimated that the amount of **S3** needed to reach insulin levels in the 250-300 pM range would be as low as ca. 210-233 µg of **S3** which is a quite low amount probably tolerable in an *in vivo* scenario.

An important issue when using delivery systems is that they should be ideally selective and deliver the cargo only in the presence of a unique target. In our case, when comparing meals of various combinations of sugars, proteins and fat, only glucose causes blood insulin levels to rise.[24] Thus, it was in our aim to demonstrate that the CD-GOx capped material **S3** is only opened in the presence of glucose and therefore control release experiments from **S3** were carried out in the presence of other

saccharides. In particular, the uncapping process in **S3** was monitored after 4 h in simulated blood plasma containing glucose, mannose, fructose, galactose or saccharose at a concentration of 10 mM. As shown in Figure 8, **S3** material shows a notable selectivity for glucose and FITC-Ins delivery from **S3** in the presence of other saccharides was irrelevant. The selective triggering of the FITC-Ins delivery is ascribed to the ability of GOx to catalyze the oxidation of glucose to gluconic acid with high specificity.

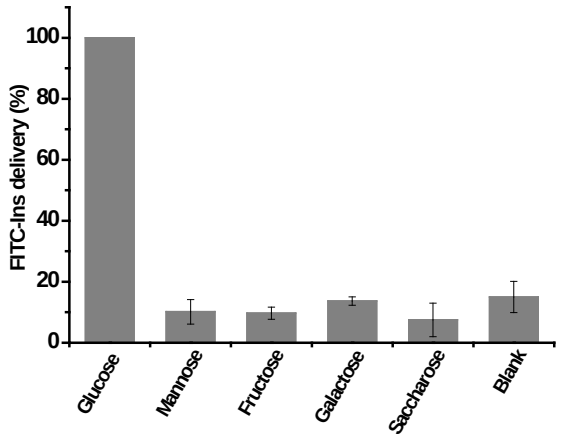

Figure 8. Release of FITC-Ins from solid **S3** in the presence of different saccharides (10 mM) after 4 h.

Conclusions

In summary, we have developed a new glucose-sensitive system for insulin controlled release. Our system consists of MSNs with an expanded pore, loaded with FITC-Ins, functionalized in the external surface with 1-propyl-1-H-benzimidazole groups and capped with CD-GOx. Conversion of glucose to gluconic acid by GOx induced the dethreading of the inclusion complexes and thus cargo release. The prepared material demonstrated to be glucose-sensitive by releasing FITC-Ins in simulated blood plasma. Moreover, the amount of delivered FITC-Ins was dependent of the concentration of glucose. Moreover, a relatively few amount of the material was able to release suitable amounts of insulin necessary to decrease the blood glucose concentration to the regular level. In addition, the system demonstrated to be highly selective and insulin delivery was only found with glucose whereas other saccharides were unable to uncap **S3**. This is one of the very few reported mesoporous supports able to release insulin triggered by the presence of glucose. Despite the fact that the road from these results to the use of nanoparticles to deliver insulin remains long and uncertain, we believe that such glucose-responsive nanoparticles able to detect levels of glucose in blood and deliver insulin accordingly may open new avenues to future designs of new drug-release system of potential application for diabetes treatment.

Experimental Section

General Techniques: Powder XRD, TG analysis, elemental analysis, TEM microscopy and N_2 adsorption-desorption techniques were used to characterize the prepared materials. X-ray measurements were performed on a Bruker AXS D8 Advance diffractometer using Cu-K_α radiation. Thermo-gravimetric analysis were carried out on a TGA/SDTA 851e Mettler Toledo equipment, using an oxidant atmosphere (Air, 80 mL/min) with a heating program consisting on in a heating ramp of 10° per minute from 273 to 373 K followed by an isothermal heating step at this temperature for 60 min in a nitrogen atmosphere (80 mL min^{-1}). Then, the program was allowed to continue with a dynamic heating segment from 373 to 1273 K in an oxidant atmosphere (air, 80 mL min^{-1}) and with an isothermal heating step at this temperature for 30 min. TEM images were taken with a JEOL TEM-1010 Electron microscope working at 100 kV. FSEM images and EDX analysis were performed with a Zeiss Ultra-55 FESEM. N_2 adsorption-desorption isotherms were recorded on a Micromeritics ASAP2010 automated sorption analyser. The samples were degassed at 120 ºC in vacuum overnight. The specific surfaces areas were calculated from the adsorption data in the low pressures range using the BET model. Pore size was determined following the BJH method. Fluorescence spectroscopy was carried out on a Jasco FP-8300 Spectrometer.

Chemicals: The chemicals *n*-cetyltrimethylammonium bromide (CTAB), sodium hydroxide (NaOH), fluorescein isothiocyanate (FITC), 3-iodopropyltrimethoxysilane, tetramethylorthosilicate (TMOS), 1,3,5-trimethylbenzene (TMB), benzimidazole, triethylamine, insulin human, dimethyl sulfoxide (DMSO), glucose, mannose, fructose, galactose, maltose and saccharose were provided by Aldrich. Analytical-grade solvents were provided by Scharlab. β-Cyclodextrin-modified glucose oxidase (CD-GOx) was synthesized as previously reported.[26]

Synthesis of MSNs with large pores S0-3: The synthetic procedure of MSNs with large pores was carried out according with previous reports with slight modifications.[21] 3.94 g of CTAB and 2.28 mL 1M of NaOH were dissolved in 800 g ethanol/water (0.4/0.6 = w/w). Then 1.3 mL of TMOS were added to the solution with vigorous stirring. After 8h, the mixture was kept unstirred overnight. The resulting white precipitate was isolated by centrifugation and washed 3 times with ethanol and 3 times with distilled water to obtain solid **S0-1**. The as-synthesised silica nanoparticles **S0-1** were dispersed in 30 mL of ethanol and the mixture was sonicated for 30 min. Subsequently, 20 mL of a 1:1 mixture (v/v) of water and TMB was added to the suspension. The mixture was kept in an autoclave at 140 °C for 4 days. The resulting solid **S0-2** was isolated by centrifugation and washed 3 times with ethanol. Finally, the material **S0-2** was calcined at 550 °C using oxidant atmosphere for 5 h in order to remove the organic content and obtain the support **S0-3**.

Synthesis of fluorescein isothiocyanate-labeled insulin (FITC-Ins): Insulin human was labelled with FITC following previous reports. [10] 2.5 mL of FITC in DMSO (1 mg mL^{-1}) was added in 5 µL aliquots with gentle stirring to a sodium carbonate buffer (0.1 M, pH 9) solution containing insulin (4 mg mL^{-1}). The reaction was stirred for 2 h in dark and at room temperature. Then, 2.5 mL of NH_4Cl 1M was added to the reaction in order to quench the excess of FITC. After stirring for an extra hour, the solution was dialyzed in phosphate-buffered saline and freeze dried yielding FITC labelled insulin. By measuring the absorbance at 495 nm and 280 nm the ratio of FITC to insulin was estimated at 1.4.

Synthesis of S1: The hybrid solid **S1** was prepared by adding an excess of 3-iodopropyltrimethoxysilane (196 µL, 1 mmol) to a suspension of 500 mg of **S0-3**. Then, the suspension was stirred for 5.5 h. The resulting solid was filtered, washed with acetonitrile and dried at 70 ºC overnight. Following, 500 mg of the resulting material were suspended in a 40 mL of a saturated solution of benzimidazole in toluene at 120 ºC and containing

triethylamine (benzimidazol and triethylamine in a 1:3 proportion). The suspension was refluxed and stirred during 72 h. The resulting white solid (**S1**) was filtered off, washed with 10 mL of acetonitrile and dried at 70 ºC overnight.

Synthesis of S2: The loading of the pores was carried out by soaking 400 mg of solid **S1** in 40 mL of HCl 0.01 M containing 200 mg of the prepared FITC-Ins. The suspension was stirred for 24 h in dark. The resulting solid was filtered off to yield **S2**, washed with 2 mL of HCl 0.01 M, dried under vacuum and stored in the fridge.

Synthesis of S3: With the aim to obtain solid **S3**, 10 mg of **S2** were suspended in a CD-GOx solution (1 mL, 1.56 mg mL^{-1}) and the suspension was stirred at room temperature for 24 h. The final yellow solid (**S3**) was centrifuged (9500 rpm, 4 min, 20 ºC) and washed with deionized water at pH 7.5 five times in order to remove the residual dye and the free CD-GOx.

Release studies: In a typical experiment, 10 mg of freshly prepared **S3** solid were suspended in 1.5 mL of deionized water at pH 7.5. Subsequently, the suspension was separated in different batches of 150 µL and each one was diluted to 3 mL with a mixture of simulated human blood plasma and deionized water at pH 7.5. At a certain time, an aliquot of 0.3 mL of the suspension was separated and centrifuged (8000 rpm, 3 min). The delivered dye was registered by measuring the FITC-Ins emission in the supernatant (λ_{ex} = 495nm).

Acknowledgements

Authors thank the Spanish Government (projects CTQ2011-24355, MAT2015-64139-C4-1-R and AGL2015-70235-C2-2-R (MINECO/FEDER)) and the Generalitat Valenciana (project PROMETEOII/2014/047) for support. M.O. thanks the Universitat Politècnica de València for her FPI grant. P.D. thanks the Ministerio de Economía y Competitividad for her FPI grant (BES-2012-054066). C.C. thanks the Generalitat Valenciana for her postdoctoral contract VALi+D.

Keywords: Mesoporous silica • Glucose • Insulin • Controlled release • Molecular gates

[1] L. Nicole, C. Laberty-Robert, L. Rozes, C. Sanchez, *Nanoscale* **2014**, *6*, 6267–92.
[2] A. A. Beltrán-Osuna, J. E. Perilla, *J. Sol-Gel Sci. Technol.* **2015**, 480–496.
[3] B. G. Trewyn, I. I. Slowing, S. Giri, H. Chen, V. S. Lin, *Acc. Chem. Res.* **2007**, 846–853.
[4] M. Vallet-Regí, F. Balas, *Open Biomed. Eng. J.* **2008**, *2*, 1–9.
[5] F. Sancenón, L. Pascual, M. Oroval, E. Aznar, R. Martínez-Máñez, *ChemistryOpen* **2015**, *4*, 418-437.
[6] (a) E. Aznar, M. Oroval, L. Pascual, J. R. Murguía, R. Martínez-Máñez, F. Sancenón, *Chem. Rev.* **2016**, *116* , 561–718; (b) E. Aznar, R. Martínez-Máñez, F. Sancenón, *Exp. Opin. Drug Deliv. Rev.* **2009**, *6*, 643-655.
[7] S. Alberti, G.J.A.A. Soler-Illia, O. Azzaroni, *Chem. Commun.* **2015**, *51*, 6050–6075.
[8] C. Argyo, V. Weiss, C. Bräuchle, T. Bein, *Chem. Mater.* **2014**, *26*, 435–451.
[9] A. P. Wight, M. E. Davis, *Chem. Rev.* **2002**, *102*, 3589–3614.
[10] G. Kickelbick, *Angew. Chem. Int. Ed.* **2004**, *43*, 3102–3104.
[11] N. K. Mal, M. Fujiwara, Y. Tanaka, *Nature* **2003**, *421*, 350-353.
[12] J. Liu, C. Detrembleur, M.-C. De Pauw-Gillet, S. Mornet, C. Jérôme, E. Duguet, *Small* **2015**, *11*, 2323-2332.
[13] Q. Fu, G.V.R. Rao, L.K. Ista, Y. Wu, B.P. Andrzejewski, L.A. Sklar, T.L. Ward, G.P. Lopez, *Adv. Mater.* **2003**, *15*, 1262-1266.
[14] A. Baeza, E. Guisasola, E. Ruiz-Hernandez, M. Vallet-Regí, *Chem. Mater.* **2012**, *24*, 517-524.
[15] R. Hernandez, H.R. Tseng, J.W. Wong, J. F. Stoddart, J. I. Zink, *J. Am. Chem. Soc.* **2004**, *126*, 3370-3371.
[16] S. Niedermayer, V. Weiss, A. Hermann, A. Schmidt, S. Datz, K. Müller, E. Wagner, T. Bein, C. Bräuchle, *Nanoscale* **2015**, *7*, 7953-7964.
[17] X. Zhang, F. Li, S. Guo, X. Chen, X. Wang, J. Li, Y. Gan, *Biomaterials* **2014**, *35*, 3650-3665.
[18] K. Patel, S. Angelos, W.R. Dichtel, A. Coskun, Y.W. Yang, J.I. Zink, J.F. Stoddart, *J. Am. Chem. Soc.* **2008**, *130*, 2382-2383.
[19] R. Bhat, A. Ribes, N. Mas, E. Aznar, F. Sancenón, M.D. Marcos, J.R. Murguía, A. Venkataraman, R. Martínez-Máñez, *Langmuir* **2016**, *32*, 1195−1200.
[20] C. Yu, L. Qian, M. Uttamchandani, L. Li, S.Q. Yao, S. Q. *Angew. Chem. Int. Ed.* **2015**, *54*, 10574-10578.
[21] M. Kavruk, O. Celikbickak, V.C. Ozalp, B.A. Borsa, F. Hernandez, G. Bayramoglu, B. Salih, M.Y. Arica, *Chem. Commun.* **2015**, *51*, 8492-8495.
[22] M.M Aye, S.L. Atkin, *Drug Healthc. Patient Saf.* **2014**, *6*, 55–67.
[23] L.-Y. Chu, *Expert Opin. Ther. Patents.* **2005**, *15*, 1147–1155.
[24] J. Suckale, M. Solimena, *Frontiers Biosci.* **2008**, *13*, 7156–7171.
[25] American Diabetes Association. *Diabetes Care*, **2014**, *37*, S14–S80.
[26] J. C. Pickup, F. Hussain, N. D. Evans, N. Sachedina, *Biosens. Bioelectron.* **2005**, *20*, 1897–1902.
[27] T. G. Farmer, T. F. Edgar, N. A. Peppas, *J. Pharm. Pharmacol.* **2008**, *60*, 1–13.
[28] G. P. Carino, E. Mathiowitz, *Adv. Drug Deliv. Rev.* **1999**, *35*, 249–257.
[29] K.A. Rubeaan, M. Rafiullah, S. Jayavanth, *Expert Opin. Drug Deliv.* **2016**, *13*, 223–237.
[30] A. Verma, N. Kumar, R. Malviya, P.K. Sharma, *J Pharm.* **2014**, *2014*, 1–9.
[31] R. Mo, T. Jiang, J. Di, W. Taiac, Z. Gu, *Chem. Soc. Rev.* **2014**, *43*, 3595—3629.
[32] K. Sato, Y. Imoto, J. Sugama, S. Seki, *Langmuir* **2005**, *21*, 797–799.
[33] S. Tanna, T. S. Sahota, K. Sawicka, M. J. Taylor, *Biomaterials* **2006**, *27*, 4498–4507.
[34] W. Qi, X. Yan, J. Fei, A. Wang, Y. Cui, J. Li, *Biomaterials* **2009**, *30*, 2799–2806.
[35] K. Ishihara, M. Kobayashi, N. Ishimaru, I. Shinohara, *Polym. J.* **1984**, *16*, 625–631.
[36] Z. Wu, X. Zhang, H. Guo, C. Li, D. Yu, *J. Mater. Chem.* **2012**, *22*, 22788.
[37] P. Liu, Q. Luo, Y. Guan, Y. Zhang, *Polymer* **2010**, *51*, 2668–2675.
[38] X. Zhang, Y. Guan, Y. Zhang, *J. Mater. Chem.* **2012**, *22*, 16299.
[39] N. Akhtar, S.A. El-Safty, M.E. Abdelsalam, H. Kawarada, *Adv. Healthcare Mater.* **2015**, *4*, 2110–2119.
[40] Y. Zhao, B. G. Trewyn, I. I. Slowing, V. S.-Y. Lin, *J. Am. Chem. Soc.* **2009**, *131*, 8398–8400.
[41] W. Zhao, H. Zhang, Q. He, Y. Li, J. Gu, L. Li, H. Li, J. Shi, *Chem. Commun.* **2011**, *47*, 9459–9461.
[42] R. N. Jain, X. Huang, S. Das, R. Silva, V. Ivanova, T. Minko, T. Asefa, *Z. Anorg. Allg.Chem.* **2014**, *640*, 616-623.
[43] É. Pérez-Esteve, A. Fuentes, C. Coll, C. Acosta, A. Bernardos, P. Amorós, M. D. Marcos, F. Sancenón, R. Martínez-Máñez, J. M. Barat, *Micropor. Mesopor. Mater.* **2015**, *202*, 124–132.
[44] C. Giménez, C. de la Torre, M. Gorbe, E. Aznar, F. Sancenón, J. R. Murguía, R. Martínez-Máñez, M. D. Marcos, P. Amorós, *Langmuir* **2015**, *31*, 3753–62.
[45] C. de la Torre, I. Casanova, G. Acosta, C. Coll, M.J. Moreno, F. Albericio, E. Aznar, R. Mangues, M. Royo, F. Sancenón, R. Martínez-

Máñez, *Adv. Funct. Mater.* **2015**, *25*, 687−695.
[46] E. Aznar, R. Villalonga, C. Giménez, F. Sancenón, M. D. Marcos, R. Martínez-Máñez, P. Díez, J. M. Pingarrón, P. Amorós, *Chem. Commun.* **2013**, *49*, 6391–6393.
[47] M. Mizutani, Y. Yamada, T. Nakamura, K. Yano, *Chem. Mater.* **2008**, *20*, 4777–4782.
[48] M. H. Kim, H. K. Na, Y. K. Kim, S. R. Ryoo, H. S. Cho, K. E. Lee, H. Jeon, R. Ryoo, D. H. Min, *ACS Nano* **2011**, *5*, 3568–3576.
[49] E. P. Barrett, L. G. Joyner, P. P. Halenda, *J. Am. Chem. Soc.* **1951**, *73*, 373–380.
[50] S. Brunauer, P. H. Emmett, E. Teller, *J. Am. Chem. Soc.* **1938**, *60*, 309–319.
[51] T. Higuchi, *J. Pharm. Sci.* **1963**, *52*, 1145–1149.
[52] É. Pérez-Esteve, M. Ruiz-Rico, C. De La Torre, L. A. Villaescusa, F. Sancenón, M. D. Marcos, P. Amorós, R. Martínez-Máñez, J. M. Barat, *Food Chem.* **2016**, *196*, 66–75.
[53] A. Bernardos, E. Aznar, C. Coll, R. Martínez-Mañez, J. M. Barat, M. D. Marcos, F. Sancenón, A. Benito, J. Soto, *J. Control. Release* **2008**, *131*, 181-189.
[54] K. Radhakrishnan, S. Gupta, D. P. Gnanadhas, P. C. Ramamurthy, D. Chakravortty, A. M. Raichur, *Part. Part. Syst. Charact*. **2014**, *31*, 449.
[55] World Health Organization: World Health Organization, International Diabetes Federation, editors. Definition and diagnosis of diabetes mellitus and intermediate hyperglycemia. Report of a WHO/IDF Consultation. Geneva (Switzerland): WHO Press; 2006.
[56] C.C. Thomas, L.H. Philipson, *Med. Clin. N. Am.* **2015**, *99*, 1–16.
[57] M. J. Mattu, and Gary W. Small, M. A. Arnold, *Anal. Chem.* **1997**, *69*, 4695.

Entry for the Table of Contents

Layout 1:

FULL PAPER

A novel nanoplatform combining diagnosing and drug delivery capabilities is presented. The capped system is based on a nanometric silica support loaded with FITC-Ins and capped with CD-GOx. This nanosystem is able to release the entrapped FITC-Ins in a controlled manner due to the specific enzymatic reaction between glucose and GOx.

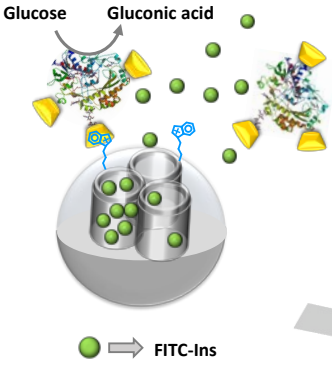

*Mar Oroval, Paula Díez, Elena Aznar, Carmen Coll, María Dolores Marcos, Félix Sancenón,Reynaldo Villalonga and Ramón Martínez-Máñez**

Page No. – Page No.

Self-regulated glucose-sensitive enzyme-capped mesoporous silica nanoparticles for insulin delivery